

Article

Spatiotemporal Effects and Optimization Strategies of Land-Use Carbon Emissions at the County Scale: A Case Study of Shaanxi Province, China

Yahui Zhang ^{1,2}, Jianfeng Li ^{3,4,*}, Siqi Liu ^{3,4} and Jizhe Zhou ⁴

¹ School of Human Settlements and Civil Engineering, Xi'an Jiaotong University, Xi'an 710049, China; baobeizhang9412@126.com

² Gansu Institute of Architectural Design and Research Co., Ltd., Lanzhou 730030, China

³ Institute of Land Engineering and Technology, Shaanxi Provincial Land Engineering Construction Group Co., Ltd., Xi'an 710021, China; 4102090209@chd.edu.cn

⁴ School of Architecture, Chang'an University, Xi'an 710064, China; jizhezhou@chd.edu.cn

* Correspondence: 2017127013@chd.edu.cn

Abstract: Land use, as one of the major sources of carbon emissions, has profound implications for global climate change. County-level land-use systems play a critical role in national carbon emission management and control. Consequently, it is essential to explore the spatiotemporal effects and optimization strategies of land-use carbon emissions at the county scale to promote the achievement of regional dual carbon targets. This study, focusing on Shaanxi Province, analyzed the spatiotemporal characteristics of land use from 2000 to 2020. By establishing a carbon emission evaluation model, the spatiotemporal effects of county-level carbon emissions were clarified. Utilizing Geodetector and K-means clustering methods, the driving mechanisms and clustering characteristics of county-level carbon emissions were elucidated, and optimization strategies for land use carbon emission were explored. The results showed that during 2000–2020, land use in Shaanxi Province underwent significant spatiotemporal changes, with constructed land increasing by 97.62%, while cultivated land and grassland were substantially reduced. The overall county-level carbon emissions exhibited a pattern of North > Central > South. The total carbon emissions within the province increased nearly fourfold over 20 years, reaching 1.00×10^8 tons. Constructed land was the primary source of emissions, while forest land contributed significantly to the carbon sink of the study area. Interactions among factors had significant impacts on the spatial differentiation of total county-level carbon emissions. For counties with different types of carbon emissions, differentiated optimization strategies were recommended. Low-carbon emission counties should intensify ecological protection and rational utilization, medium-carbon emission counties need to strike a balance between economic development and environmental protection, while high-carbon emission counties should prioritize profound emission reduction and structural transformation.

Keywords: carbon emissions; dual carbon targets; land use; county-level; Geodetector



Citation: Zhang, Y.; Li, J.; Liu, S.; Zhou, J. Spatiotemporal Effects and Optimization Strategies of Land-Use Carbon Emissions at the County Scale: A Case Study of Shaanxi Province, China. *Sustainability* **2024**, *16*, 4104. <https://doi.org/10.3390/su16104104>

Academic Editors: Luca Salvati and David Lopez-Carr

Received: 17 March 2024

Revised: 23 April 2024

Accepted: 11 May 2024

Published: 14 May 2024



Copyright: © 2024 by the authors. Licensee MDPI, Basel, Switzerland. This article is an open access article distributed under the terms and conditions of the Creative Commons Attribution (CC BY) license (<https://creativecommons.org/licenses/by/4.0/>).

1. Introduction

Global climate change has emerged as a major challenge confronting humanity [1,2]. Owing to the rapid expansion of industrialization and extensive human activities, there has been a consistent escalation in the emission of greenhouse gases, resulting in a persistent increase in worldwide temperatures, a higher frequency of extreme weather phenomena, and significant effects on human civilizations and natural ecosystems [3–5]. To address these environmental challenges and climatic alterations, in 2020, China introduced the dual objectives of achieving a carbon peak and advancing toward carbon neutrality [6]. Being the largest global contributor to carbon dioxide emissions, China's endeavors in reducing emissions are of paramount importance to the global mitigation efforts [7]. Shaanxi

Province, as the leading province by Gross Domestic Product (GDP) in China's northwest region and possessing energy reserves that rank among the nation's most substantial, plays a critical role in influencing China's overall emission reduction efforts through its carbon emission profile and associated reduction strategies [8]. Land-use change is recognized as one of the most direct anthropogenic drivers affecting the terrestrial ecosystem carbon cycle, contributing to approximately one-third of human-induced carbon emissions [9]. Counties, serving as critical administrative units that bridge overarching strategies with practical implementations [10], urgently require in-depth research into the spatiotemporal effects of land use on carbon emissions and optimization strategies at the county scale. Such research endeavors are crucial for a comprehensive understanding of the distribution patterns, regional disparities, and driving factors of carbon emissions, enabling the implementation of targeted, refined reduction measures at smaller scales.

Land use plays a crucial role in shaping the carbon footprint of human activities [11,12]. Alterations in land use predominantly exert influence on the carbon cycle dynamics within ecosystems through modifications in both their structural attributes (species constitution and biomass) and functions (biodiversity, energy equilibrium, and carbon circulation processes) [13]. On the one hand, as the natural spatial carrier for terrestrial ecosystem carbon sources/sinks, alterations to the scale, structure, layout, and intensity of land use directly or indirectly cause variations in carbon emissions/sequestration [14]. On the other hand, as socio-economic carriers of human production and life, land bears the brunt of substantial carbon emissions from socio-economic activities [15]. Significant differences in carbon emissions exist under different land-use types [16]. Grassland, forest, shrubland, and wetland are identified as major carbon sinks, whereas construction land and cultivated land are recognized as primary carbon sources [17]. The basis of research on carbon emissions from land use rests on the accounting of carbon emissions, and currently, the main methods include field measurements [18], carbon emission coefficient method [19], model calculations [20], and remote sensing estimation [21]. Among these, the carbon emission coefficient method, due to its simplicity, practicality, and broad applicability, has been widely adopted [19,22]. Building upon carbon emission accounting, scholars have conducted studies at various scales and perspectives, focusing on aspects like carbon emission intensities [23], spatiotemporal variations [24], evolutionary patterns [25], driving factors [26], and optimization strategies [27]. The spatiotemporal effects, driving mechanisms, and optimization methods of land-use carbon emissions are current hotspots in research [28–30]. In the field of spatiotemporal effect research, scholars mainly focus on the changes in land-use types, the dynamic balance between carbon sources and carbon sinks, regional differences, and evolutionary characteristics [31], with investigative scopes encompassing multiple scales ranging from global [32] to national [33], provincial [34], city clusters [35], and urban areas [36]. The focus has predominantly been on macro scales, while research at the county level remains relatively scarce. Addressing this gap, the current study zeroes in on Shaanxi Province, comprehensively analyzing the spatiotemporal distribution and evolution of land-use carbon emissions specific to its counties. In terms of land-use carbon emission driving factors, traditional econometric methods like the logarithmic mean division index (LMDI) decomposition method [37], stochastic impacts by regression on population, affluence, the technology (STIRPAT) model [38], and the grey correlation model [39] are commonly used, but often fail to consider spatial differences among influencing factors and the interactive effects of these factors on the spatial differentiation of land-use carbon emissions, thereby not fully elucidating the drivers behind spatial disparities. Geodetector [40], by contrast, offers a more robust mechanism for detecting and quantifying the distinct contributions and interplays of diverse factors affecting the spatial variance in land-use carbon emissions, thus facilitating a deeper exploration of the intricate causal networks embedded within

spatial datasets. Regarding land-use carbon emission optimization, regional discrepancies and ecological complexity limit the generalizability of existing findings [41]. Moreover, the complexity of land-use policy implementation and insufficient consideration of socio-economic factors impede a comprehensive understanding of the multifaceted influences on carbon emission optimization [27,42]. Current optimization outcomes are not readily applicable at the county level, necessitating more localized, nuanced research and strategy formulation that better accommodates local characteristics, policy practices, and socio-economic contexts. There exists an acute necessity to delve into the effective translation of the dual carbon objectives into concrete land-use units, thereby steering spatial planning and development via carbon emission abatement, which is yet to be thoroughly investigated.

This study is dedicated to revealing the spatiotemporal effects of land-use carbon emissions at the county level and exploring effective optimization pathways to achieve dual carbon targets. Through an in-depth examination of the dynamic changes and optimization of land-use carbon emissions across 107 counties in Shaanxi Province, the aim is to elucidate the characteristics of land-use change and transfer, spatiotemporal effects of carbon emissions, and driving mechanisms at the county level, and propose tailored emission reduction strategies for counties exhibiting distinct clustering attributes. The outcomes of this research are poised to facilitate the advancement of emission mitigation and carbon sequestration across diverse types of land utilization, steering regional economies towards a path of low-carbon metamorphosis and sustainable growth.

2. Materials and Methods

2.1. Study Area

Located in the heart of China, Shaanxi Province holds substantial geographical, ecological, and economic significance, serving as a key player in the strategic “Belt and Road” initiative [43]. The province boasts a diverse landscape characterized by a topographic gradient that descends from elevated northern and southern territories towards the central lowlands, generally classified into three primary geographic regions: the Loess Plateau, the Weihe Plain, and the QinBa Mountain. This array of unique terrains, geomorphological features, climatic conditions, and natural endowments has engendered significant economic disparity within Shaanxi. The northern section of the province is renowned for its copious energy resources, with the energy industry exercising considerable sway. This region’s coal and oil production figures rank amongst the nation’s highest, making substantial contributions to the energy needs not only of Shaanxi but also the broader national context. By contrast, Central Shaanxi represents the economic nucleus of the province, commanding the largest GDP and boasting a multifaceted industrial setup that encompasses conventional agriculture, cutting-edge manufacturing, contemporary service sectors, as well as high-tech industries. The southern area, recognized for its extensive natural reserves, is focusing on eco-tourism development, harnessing its unique environmental qualities as precious assets for its eco-tourism market. It is pertinent to mention that about 93% of China’s carbon emissions are attributed to the consumption of fossil fuels. As a major energy-producing province with the third-highest coal output and the first-ranked equivalent of oil and gas production nationwide, Shaanxi faces considerable challenges in controlling carbon emissions. Furthermore, given the imperative for energy structure transformation and the pursuit of green development, Shaanxi must actively explore low-carbon and sustainable development pathways while ensuring economic growth. The study area’s location is depicted in Figure 1.

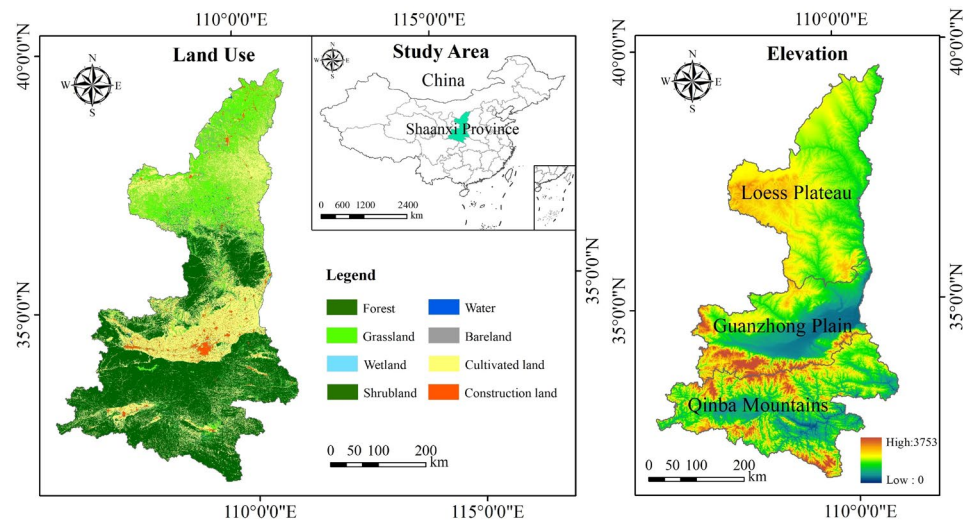


Figure 1. Location of the study area.

2.2. Data

This study utilized seven distinct types of data, specifically encompassing land use, population, nighttime light imagery, the vegetation index, GDP, carbon emission, and the administrative boundary. Table 1 provides detailed information on all the data used. The GlobeLand30 data, featuring a 30 m resolution, was predominantly utilized for scrutinizing changes in land use and computing two pivotal factors: land-use intensity and the per capita area of construction land. Worldpop data [44], NPP-VIIRS-like nighttime light data [45], MOD13Q1, and 1 km grid GDP data of China [46] were utilized for determining population density, nighttime light intensity, annual average normalized difference vegetation index (NDVI), and per capita GDP, respectively. To surmount the challenges posed by years of administrative boundary changes and discrepancies in statistical standards, WorldPop data have been utilized instead of official census data to ensure the integrity and continuity of population data analysis. The WorldPop dataset integrates census data with multiple sources of information, including land cover, nighttime light, and topography, and has been widely adopted across various disciplines such as social sciences and geosciences [44]. Furthermore, the Open-source Data Inventory of Anthropogenic CO₂ Emissions (ODIAC) [47] was employed for estimating carbon emissions associated with construction land use. It is important to highlight that, in the data processing phase, we utilized the resampling functionality within ArcGIS 10.3 software to resample the spatial resolution of the data to 100 m.

Table 1. The detailed information of databases.

Data Type	Year	Resolution (m)	Download Link
GlobeLand30	2000, 2010, 2020	30	http://www.globallandcover.com (accessed on 2 August 2023)
Worldpop	2000, 2010, 2020	100	https://www.worldpop.org.uk (accessed on 10 October 2023)
NPP-VIIRS-like NTL data	2000, 2010, 2020	500	http://nnu.geodata.cn/data (accessed on 12 October 2023)
MOD13Q1	2000, 2010, 2020	250	https://ladsweb.modaps.eosdis.nasa.gov/search (accessed on 15 October 2023)
1 km grid GDP data of China	2000, 2010, 2020	1000	https://www.resdc.cn/ (accessed on 20 October 2023)
ODIAC	2000, 2010, 2020	1000	https://db.cger.nies.go.jp (accessed on 24 October 2023)
Administrative boundary	2020	\	http://www.dsac.cn/ (accessed on 10 August 2023)

3. Methodologies

This study's technical flowchart was delineated into four primary steps, as illustrated in Figure 2. In the initial step, the spatiotemporal change characteristics of land use were examined. Based on the GlobeLand30 data spanning from 2000 to 2020 for Shaanxi Province, temporal variations and spatial transitions among different land-use types within the study area were scrutinized using geostatistical tools in ArcGIS and the transition matrix method. The second step involved scrutinizing the spatiotemporal dynamics of carbon emissions from land use. A model for estimating land-use carbon emissions was formulated by referencing pertinent research [48] while ensuring the precision and availability of actual data. Specifically, direct carbon emission coefficients were utilized to quantify emissions from forest, grassland, cultivated land, shrubland, wetland, water, and bareland. For construction land, carbon emissions were estimated using ODIAAC data. The third step entailed identifying the driving factors influencing land-use carbon emissions. In consideration of data accessibility and precision, and drawing upon the foundation of existing research [49,50], our study thoughtfully selected six key indicators to construct the driving factor indicator system. These indicators were chosen for their significant impact on land use and environmental change, including I (population density), II (per capita GDP), III (land-use intensity), IV (nighttime light intensity), V (NDVI), and VI (per capita construction land area). GeoDetector's factor detector and interaction detector were further applied to scrutinize the underlying drivers of spatial heterogeneity in land-use carbon emissions at the county scale. Finally, in the fourth step, clustering and optimization strategies for county-level land-use carbon emissions were investigated. The K-means clustering algorithm was employed to categorize and summarize the carbon emission status across counties. Tailored optimization strategy recommendations were then proposed for each cluster based on the unique characteristics of land-use carbon emissions within those clusters. It should be noted that this study evaluated the temporal changes and spatial transitions of land use in Section 4.1, explored the spatiotemporal effects of county-level carbon emissions in Section 4.2, and clarified the underlying drivers of spatial differentiation for land-use carbon emissions in Section 4.3. Based on the analyses above, in the Discussion section, this study investigated the clustering characteristics and optimization strategies for land-use carbon emissions at the county level.

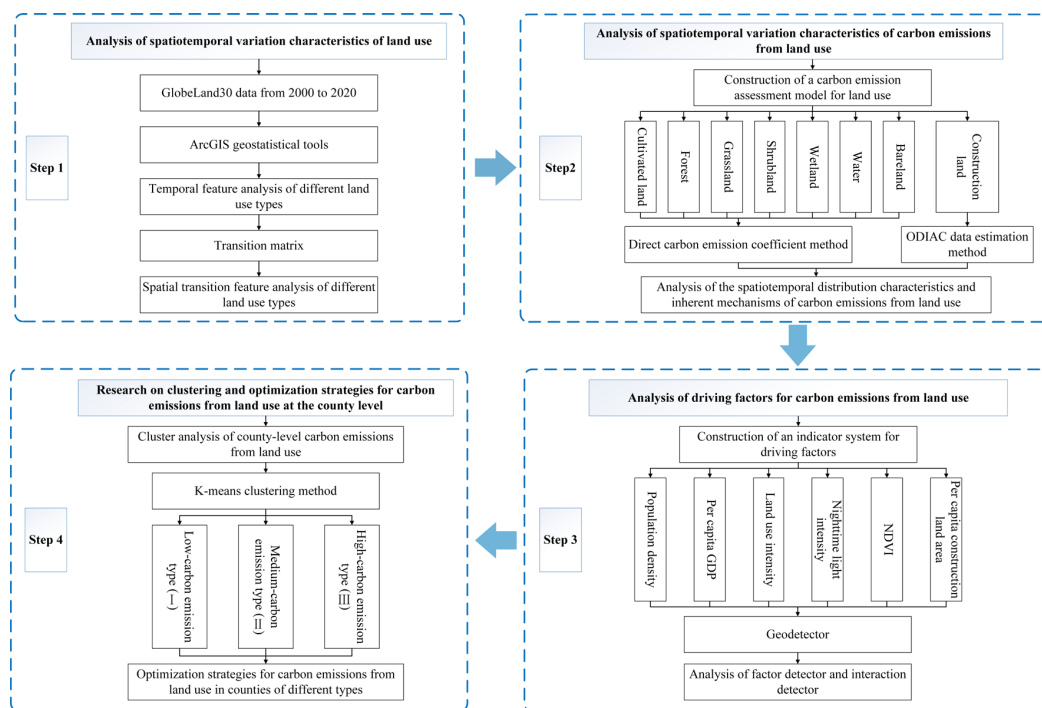


Figure 2. Technical flowchart.

3.1. Land Use Carbon Emission Estimation Model

Carbon emissions from land use encompass both direct and indirect emissions [51]. Direct carbon emissions specifically arise from land use activities, while indirect emissions predominantly result from the aggregate of anthropogenic carbon emissions associated with diverse land-use types. Cultivated land, forest, grassland, shrubland, wetland, water, and bareland are typically evaluated using direct carbon emission coefficients, whereas construction land is assessed through indirect carbon emission estimation methods. Carbon emissions from construction land are commonly represented by the volume of CO₂ produced from energy consumption in industrial and daily life processes. Given the lack of long-term county-level energy consumption statistics for Shaanxi Province, this study utilized monthly fossil fuel emission data from ODIAC [47] to estimate carbon emissions from construction land.

The direct carbon emission coefficient method can be expressed as follows:

$$E_k = \sum e_i = \sum T_i \delta_i \quad (1)$$

where E_k represents the direct carbon emissions, e_i signifies the emissions from land use type i , T_i represents the total area of the land use type i , and δ_i is the coefficient for carbon emissions associated with land use type i . Coefficients for carbon emissions of various land use categories have been established with reference to the extant literature, as delineated in Table 2.

Table 2. The carbon emission coefficients for different land-use types.

Land Use Type	Carbon Emission Coefficients (kg·m ⁻² ·a ⁻¹)
Cultivated land	0.0422 [17]
Forest	−0.0644 [17]
Grassland	−0.0022 [17]
Shrubland	−0.02300 [52]
Wetland	−0.000006132 [53]
Water	−0.0253 [54]
Bareland	−0.0005 [55]

The formula employed in this study to calculate carbon emissions from construction land is as follows:

$$E = \sum E_i \quad (2)$$

where E represents the total indirect carbon emissions, and E_i is the carbon emission amount for month i as recorded in the ODIAC dataset. This study established a land-use carbon emissions assessment model through the amalgamation of the direct carbon emission coefficient method with the construction land carbon emission calculation method (Formula (2)), thus effectively circumventing the challenge of missing long-term energy statistical data.

3.2. Geodetector

The Geodetector comprises a suite of statistical tools tailored for identifying spatial heterogeneity and discerning the driving mechanisms beneath [40]. It encompasses several modules: the factor detector, the risk detector, the interaction detector, and the ecological detector. The goal of the factor detector is to investigate the spatial variability of the dependent variable Y and to quantify the explanatory power of an independent factor X on Y , represented by the q value. The equation to calculate q is presented below:

$$q = 1 - \frac{\sum_{h=1}^L N_h \sigma_h^2}{N \sigma^2} = 1 - \frac{SSW}{SST} \quad (h = 1, 2, \dots) \quad (3)$$

$$SSW = \sum_{h=1}^L N_h \sigma_h^2, \quad SST = N \sigma^2$$

where L denotes the stratification or categorization of variable Y or factor X ; h represents the count of partitions or classifications of Y or factor X ; N_h and N are the number of units in class h and the entire region, respectively; σ^2 and σ_h^2 are the variances of Y in the entire study area and class h , respectively; and SSW and SST , respectively, represent the within-class sum of squares and the overall total sum of squares. The q -statistic varies from 0 to 1, and as its magnitude increases, it indicates a heightened spatial variation in the attribute Y . When partition h arises from factor X , a higher q -value conveys that factor X has a more impactful effect on the variable Y . Conversely, a smaller q suggests that its explanatory power over variable Y is less pronounced.

The interaction detector is employed to evaluate the combined effect between factors X_i and X_j , reflecting how their joint influence either enhances, weakens, or acts independently on the variable Y . This process typically involves calculating the explanatory power, denoted as $q(X_1)$ and $q(X_2)$, of the two influencing factors X_i and X_j on the attribute Y independently. Subsequently, the interaction value $q(X_1 \cap X_2)$ is computed. The risk detector is used to ascertain whether there is statistical significance in the average attributes across different regions. The ecological detector's function is to ascertain the presence of substantial variances in the impacts that different determinants have on the spatial distribution of attribute values. In this study, the factor and interaction detectors were utilized to investigate the driving forces of carbon emissions originating from land use at the county scale.

3.3. K-Means Clustering Algorithm

The K-Means clustering algorithm, an unsupervised clustering technique, is designed to partition a dataset into K clusters, emphasizing tight intra-cluster connectivity and maximal separation between distinct clusters [56]. The primary goal is to categorize samples into mutually exclusive clusters, where high intra-cluster similarity prevails, and low inter-cluster similarity exists. To compute the Euclidean separation between spatial data entities and their respective cluster centroids, the following equation is employed:

$$d(X, C_i) = \sqrt{\sum_{j=1}^m (X_j - C_{ij})^2} \quad (4)$$

where X is the data objects, C_i represents the i -th cluster center, m represents the dimensionality of the data object, and X_j and C_{ij} denote the j -th attribute values of X and C_i , respectively. The aggregate sum of squared error (SSE) across the entire dataset can be computed using the following mathematical expression:

$$SSE = \sum_{i=1}^k \sum_{X \in C_i} |d(X, C_i)|^2 \quad (5)$$

where the magnitude of SSE signifies the clustering outcome's quality, and k denotes the total number of clusters.

4. Results

4.1. Spatiotemporal Analysis of Land-Use Change

Figure 3 illustrates the changes in area and change rates of different land-use types from 2000 to 2020. The figure revealed significant disparities in the area changes among different land-use categories. Construction land, forest, shrubland, and water demonstrated an ascending trend, with the degree of increase ranked as follows: construction land > shrubland > water > forest. Notably, there was a significant expansion in construction land, escalating from 3338.24 km² to 6597.07 km², reflecting a remarkable growth rate of 97.62%. Similarly, shrubland exhibited a rapid increment, growing by 59.30%. In contrast, cultivated land, grassland, wetland, and bareland manifested a decreasing tendency, with the magnitude of decrease ordered as follows: wetland > bareland > grassland > cultivated

land. Of particular significance, both cultivated land and grassland areas experienced reductions exceeding 1500 km².

Through analyzing the spatial distribution pattern of land use in Shaanxi Province from 2000 to 2020 (Figure 4) and the characteristics of land-use changes (Tables 3 and 4), it was found that the dominant land-use types in Shaanxi Province were cultivated land, forest, and grassland, with their combined area exceeding 95% of the total provincial area. Land-use transitions primarily occurred among these three land uses and construction land. The ranking of land-use types based on their area was as follows: forest > cultivated land > grassland > construction land > bareland > water > shrubland > wetland. From 2000 to 2020, the total transfer area among various land-use types in Shaanxi Province amounted to 26,381.26 km². Among these, the transferred areas from cultivated land, forest, and grassland accounted for 35.13%, 21.30%, and 33.76% of the total transferred area, respectively, while the remaining land-use types contributed only 9.81%. Cultivated land was mainly distributed in the Guanzhong Plain (in Weinan, Xianyang, and Baoji cities) and certain regions of the Loess Plateau in Shanbei (specifically in Yulin City). Over the 20-year period, cultivated land experienced the largest transfer, amounting to 9266.57 km², predominantly converting to construction land, grassland, and forest. The conversion of cultivated land to construction land was concentrated in the Guanzhong region and along the Hanjiang River Basin urban agglomerations, whereas transfers to grassland and forest mainly took place in the northern Loess Plateau and the river valley areas of the Qinba Mountains in Shannan. Forest was concentrated mainly in the Qinba Mountains and the central-northern Loess Plateau region (including Huanglong Mountain and Ziwu Mountain). The Qinba Mountains are abundant in water resources and boast an exceptionally high forest coverage rate, serving as a crucial ecological security barrier in China, with vital functions such as biodiversity conservation and water retention. The land-use types in the Ziwu Mountain and Huanglong Mountain areas are largely consistent with those in the Qinba Mountains, featuring comparably high vegetation cover. From 2000 to 2020, approximately 5621.95 km² of forest was converted from cultivated land and grassland, representing 98.69% of the total forest expansion. Grassland was predominantly located in the Loess Plateau region of Shanbei. Over the 20-year period, grassland transitioned to cultivated land by 4086.25 km² and to forestland by 3108.97 km². With the continuous advancement of urbanization and industrialization processes, construction land expanded rapidly during 2000–2020, especially in the urban agglomerations of the Guanzhong Plain. The expansion of construction land was primarily sourced from cultivated land, contributing to 78.22% of the total construction land increase.

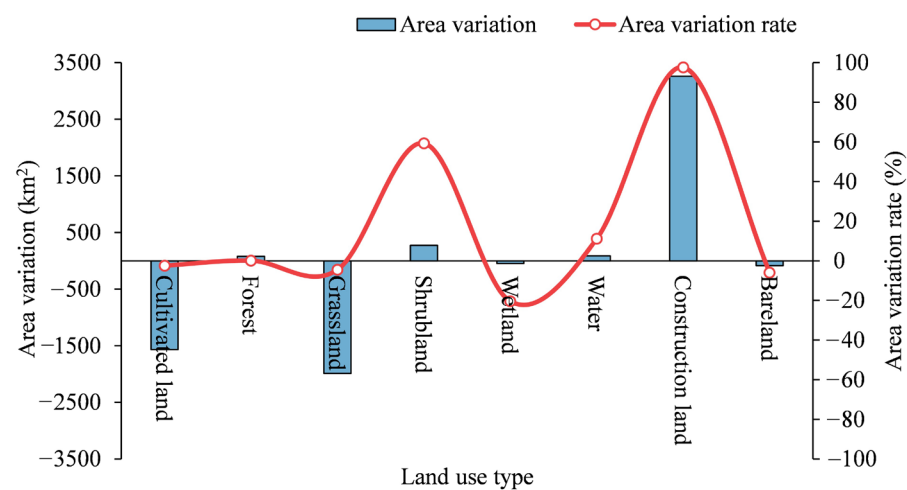


Figure 3. The changes in area and change rates of various land-use types from 2000 to 2020.

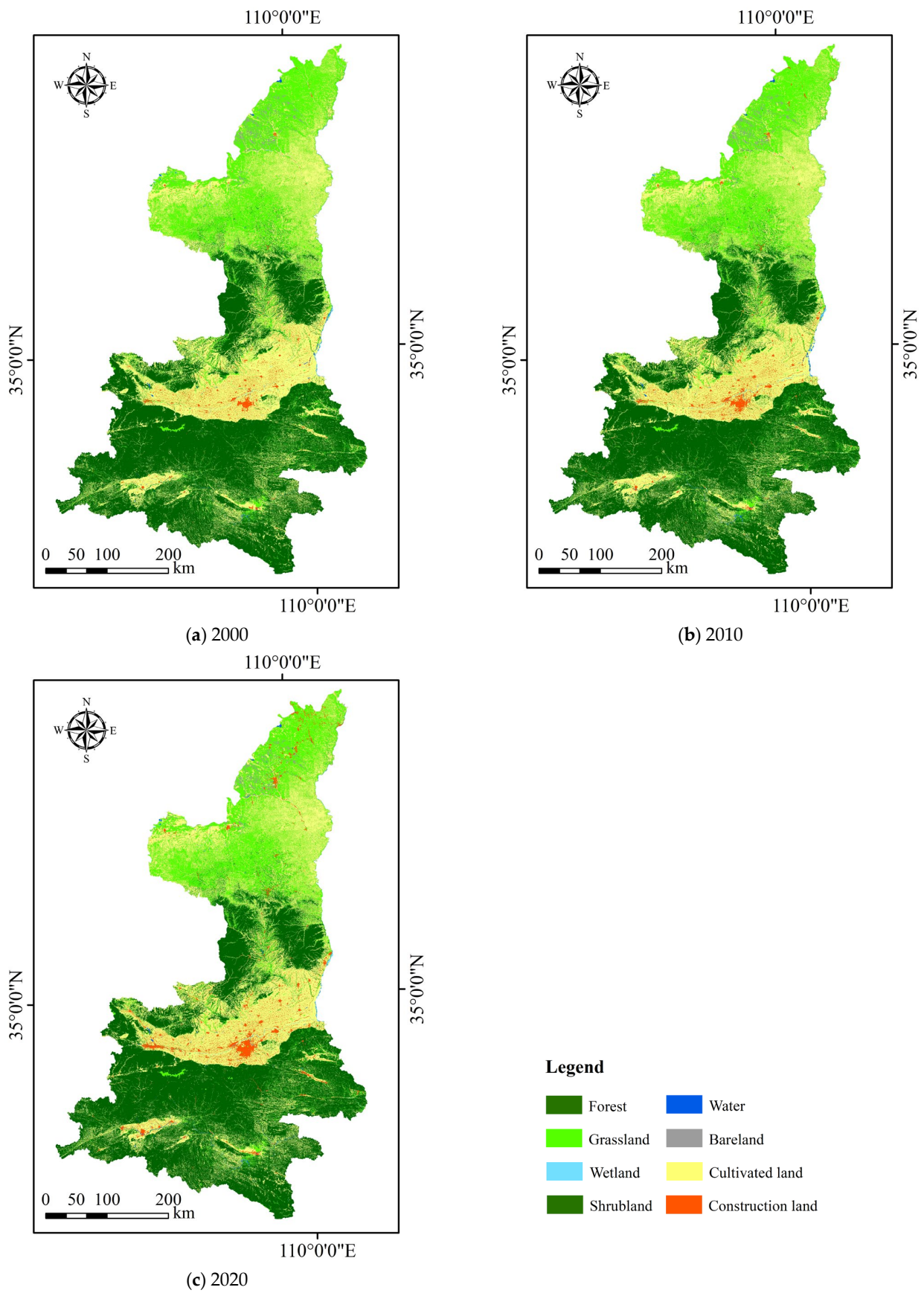


Figure 4. The land-use distribution pattern from 2000 to 2020.

Table 3. The total area of different land-use types from 2000 to 2020. (km²).

Year	Cultivated Land	Forest	Grassland	Shrubland	Wetland	Water	Construction Land	Bareland
2000	64,148.62	91,486.90	44,172.23	458.97	247.33	759.57	3338.24	1453.15
2010	63,141.59	91,790.55	43,416.98	763.23	209.79	789.04	4486.25	1467.58
2020	62,580.83	91,566.22	42,182.08	731.14	196.73	844.08	6597.07	1366.86

Table 4. The transition matrix of land use in Shaanxi Province from 2000 to 2020 (km²).

2020 \ 2000	Cultivated Land	Forest	Grassland	Shrubland	Wetland	Water	Construction Land	Bareland
Cultivated land	54,878.04	2512.98	3253.37	84.41	32.26	188.73	3168.40	26.42
Forest	2453.69	85,852.26	2837.83	114.77	4.02	124.43	80.11	5.56
Grassland	4086.25	3108.97	35,259.45	435.71	20.62	99.71	725.79	428.01
Shrubland	57.60	21.12	283.99	86.84	0.14	2.32	4.82	1.95
Wetland	75.56	3.58	27.12	0.45	83.72	44.74	4.48	6.76
Water	180.90	37.36	75.91	3.85	54.30	373.20	21.19	7.78
Construction land	749.35	9.50	25.96	0.63	0.08	6.10	2546.32	0.29
Bareland	95.62	3.00	413.27	4.30	0.03	0.57	45.70	889.85

4.2. County-Level Spatiotemporal Effects Analysis of Land-Use Carbon Emissions

Analyzing the carbon emissions from land use at different time periods (Table 5), it was evident that Shaanxi Province qualifies as a carbon source region. From 2000 to 2020, its carbon emissions exhibited a significant upward trend, surging from 2.65×10^7 t to 1.00×10^8 t, representing an almost fourfold increase. This growth trajectory can be delineated into two phases: a period of rapid increase (2000–2010) and a period of gradual growth (2010–2020). Among various land-use types, forests emerged as the predominant carbon sink, contributing over 97% to the total carbon sink and playing a pivotal role in regional carbon uptake. In contrast, cultivated land consistently experienced a gradual reduction in carbon emissions, constituting 9.08% of total emissions in 2000, 3.26% in 2010, and 2.53% in 2020. Conversely, construction land served as the primary carbon source, contributing significantly to the overall carbon emissions resulting from land-use activities. The substantial increase in carbon emissions from these construction lands stood out as the principal factor propelling the noteworthy overall surge in carbon emissions within the study area during this period.

Table 5. Land-use carbon emissions in Shaanxi Province from 2010 to 2020 ($\times 10^4$ t).

Year	Carbon Source		Carbon Sink						Total Carbon Emissions
	Cultivated Land	Construction Land	Forest	Grassland	Shrubland	Wetland	Water	Bareland	
2000	270.6975	2982.3491	−589.1127	−9.7170	−1.0554	−0.0002	−1.9140	−0.0726	2651.1747
2010	266.4473	8173.5850	−591.0677	−9.5509	−1.7551	−0.0001	−1.9889	−0.0734	7835.5962
2020	264.0798	10,425.9585	−589.6232	−9.2792	−1.6813	−0.0001	−2.1289	−0.0683	10,087.2573

The spatial distribution pattern of county-level land-use carbon emissions in Shaanxi Province between 2000 and 2020 (depicted in Figure 5a–c) revealed outstanding spatial heterogeneity in total carbon emissions among counties, presenting an overall gradient of northern > central > southern regions, along with distinct temporal variations over the period. Regions with high-value carbon emissions are predominantly concentrated in the northern and northwestern parts of the Shanbei region and some areas in the Guanzhong Plain. Conversely, regions with low-value emissions were mainly found in the Qinba Mountains of Shannan and the middle-northern Loess Plateau. Over the 20-year period, all counties experienced increases in total carbon emissions, with particularly pronounced growth occurring between 2000 and 2010. From 2000 to 2020, there was a dramatic decrease

in the number of counties that were overall carbon sinks, declining from 28 to 12, primarily located in the Shannan region. Conversely, there was a substantial increase in the number of counties where carbon emissions exceeded 5×10^5 t, rising from 14 to 44, primarily concentrated in energy-rich counties of Shanbei and those with higher urbanization levels in the Guanzhong area.

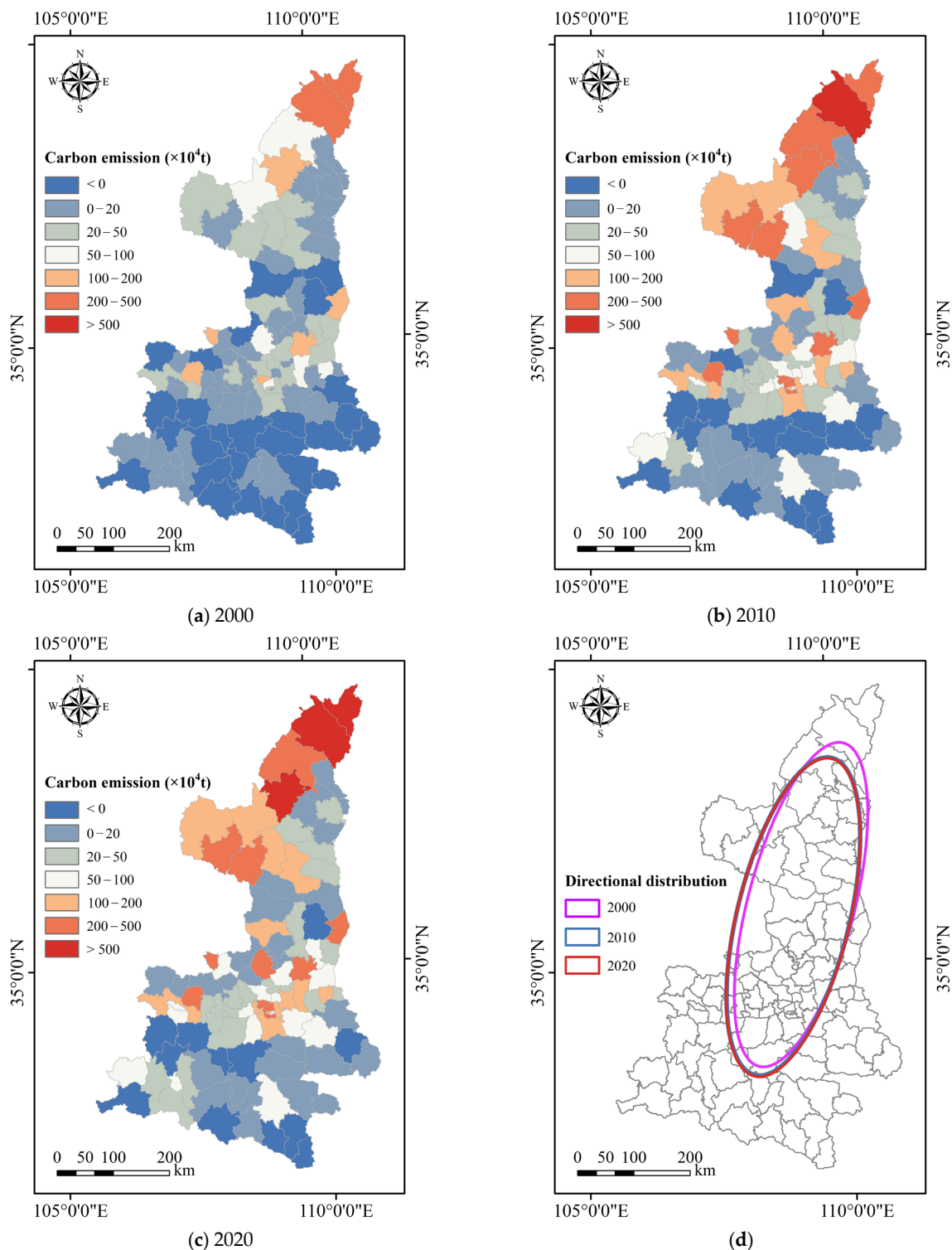


Figure 5. (a–c) represent the total land-use carbon emissions at the county level in the study area for the years 2000, 2010, and 2020, respectively. (d) characterizes the directional features of spatial distribution of land-use carbon emissions in the study area for the years 2000, 2010, and 2020.

Based on the spatial differentiation pattern revealed by the standard deviation ellipse analysis (Figure 5d), the overall carbon emission distribution in Shaanxi Province was predominantly oriented along a northeast-southwest axis, with an observed trend of the spatial distribution center shifting towards the southwest and an expansion of the spatial distribution range. From 2000 to 2020, the spatial center of land-use carbon emissions in Shaanxi moved 27.50 km from the northeast to the southwest, with the most pronounced movement occurring between 2000 and 2010, amounting to 25.77 km. During 2000–2010, there was a noticeable trend of increasing ratios between the minor and major axes of the standard deviation ellipse representing the spatial distribution of carbon emissions across the province. Subsequently, from 2010 to 2020, these ratios remained relatively constant. In terms of shape differentiation, the azimuth of the standard deviation ellipse for carbon emissions in the province continuously narrowed from 15.19° in 2000 to 14.18° in 2020, indicating an enhanced impact of the southwestern region of Shaanxi Province on the spatial pattern of carbon emissions over the 20-year period.

4.3. Analysis of Driving Factors for Spatial Differentiation of Carbon Emissions

To unravel the mechanisms driving the spatial differentiation of county-level carbon emission totals in the study area, we employed Geodetector to conduct analyses on factor detection and interaction detection, exploring the spatial heterogeneity of carbon emissions. The results obtained from the factor detector revealed the individual explanatory capacities of each factor in accounting for the spatial disparities of carbon emission totals at the county scale, represented by the parameter q . A heightened q -value signifies that the factor exercises a more substantial impact on the spatial patterning of carbon emissions within counties. Analysis of the results of the factor detector (Figure 6a) revealed that the ranking of the explanatory power of different factors for the spatial heterogeneity of county-level carbon emissions in Shaanxi Province was as follows: per capita GDP (II) > nighttime light intensity (IV) > land-use intensity (III) > per capita construction land area (VI) > population density (I) > NDVI (V). The q -values for per capita GDP, nighttime light intensity, land-use intensity, and per capita construction land area exceeded 0.32, signifying the significant impact of these four factors on the spatial distribution pattern of county-level carbon emissions. Per capita GDP can reflect the level of economic development in a region, with higher energy consumption and carbon emissions generally corresponding to more advanced economic development [57]. Given the considerable economic development disparities across Shaanxi Province, per capita GDP exhibited a strong explanatory power for the spatial variation of county-level carbon emissions. In regions with higher urbanization levels and economic development, night-time light intensity tends to be greater [58,59]. These areas typically host more intense economic and human activities, likely leading to elevated carbon emissions. Land-use intensity reflects the degree of development and utilization of land resources, with variations in land resource utilization across different counties. Higher land-use intensity often signifies increased energy consumption. During the rapid urbanization process, the total area of construction land has been continually expanding, particularly the construction of new residential areas, factories, and commercial facilities, which has led to an increase in carbon emissions.

The interactive detection method was pivotal for unraveling the complex synergies among various determinants that drive the patterns of spatial variance in county-level carbon emissions. Examination of the results from interactive detection (Figure 6b) indicated that the interplay among factors consistently exhibited amplification, either bilinear or nonlinear, without any evidence of neutral or diminishing interrelations. Specifically, except for the interaction between per capita GDP and the three factors of land-use intensity, nighttime light intensity, and per capita construction land area, which exhibited a bilinear enhancement, the interactions among the remaining factors were all characterized by nonlinear enhancement. The q -values associated with the interactions between different factors were notably greater than the q -values for individual factors. The majority of interaction q -values between factors surpassed 0.6, constituting over 93% of the total considered

interactions. The interplay between nighttime light intensity and per capita construction land area showcased the highest q -value, having reached 0.8455. The minimum interaction q -value was noted for the interplay between population density and NDVI, reaching 0.5434, yet this value still exceeded the maximum q -value for any single factor. The experimental results highlighted that the explanatory power of interactive effects among factors for the spatial variation in county-level carbon emissions was enhanced to varying degrees compared to individual factor effects. Each combination of interactions between different factors exerted distinct influences on the spatial differentiation of total carbon emissions.

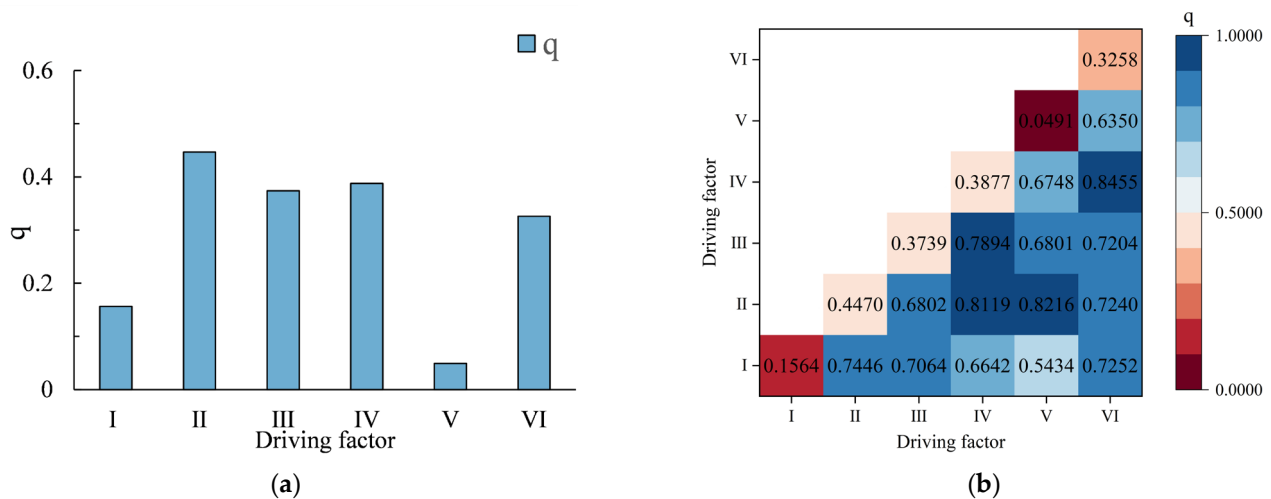


Figure 6. (a) Results of the factor detector (except for the significance factor p of NDVI, which was greater than 0.05, all other factors were less than 0.05). (b) Results of the interaction detector.

5. Discussion

5.1. Optimization Strategies for Land-Use Carbon Emissions under Dual Carbon Targets

Amidst the escalating severity of global climate change, carbon emissions have become a pivotal factor impacting human survival and development [60]. Land use, as one of the major sources of carbon emissions, its optimization strategies are of crucial significance for achieving dual carbon goals [20]. County-level land-use systems, acting as a crucial tier in national carbon emission management and control, bear essential responsibilities by embodying overarching layout requirements from higher levels and guiding specific implementations at lower administrative divisions [10]. In the pursuit of dual carbon targets, a fundamental step involves improving and optimizing land-use patterns to facilitate low-carbon economic and social transformation and attain sustainable development objectives [61]. Current strategies for optimizing carbon emissions related to land use predominantly focus on multi-dimensional influencing factors, including adjustments to land-use types, reforms in industrial structures, improvements in energy consumption efficiency, and planning urban-rural construction layouts [27]. However, these strategies have yet to fully integrate spatial configurations of carbon sink potential, particularly lacking refined research tailored to different county scales. Within Shaanxi Province, distinct spatial variations in geographical features, economic development models, and land-use patterns contribute to unique characteristics among various types of counties in terms of land-use structures, the distribution of emission sources, and the spatiotemporal dynamics of total carbon emissions. Consequently, the formulation of tailored carbon emission optimization strategies for different types of counties is of paramount importance.

Based on the 2020 county-level land-use carbon emission results in Shaanxi Province, the carbon emission proportions for various land-use types in each county were computed. Range normalization was applied to standardize the data, followed by the utilization of K-means clustering for the categorization of counties. The K-means algorithm ensured that the proportions of carbon emissions for different land-use types are most similar,

maximizing their resemblance. According to the clustering results, Shaanxi Province's counties can be categorized into low-carbon emission (Type I), medium-carbon emission (Type II), and high-carbon emission (Type III) (Table 6 and Figure 7).

Table 6. Clustering results of county-level land-use carbon emissions in Shaanxi province in 2020.

Emission Type	Number	Proportion (%)	County Name
Low-carbon emission (Type I)	14	13.08	Danfeng County, Feng County, Foping County, Huanglong County, Langao County, Liuba County, Linyou County, Ningshan County, Ningqiang County, Pingli County, Taibai County, Zhen'an County, Zhenba County, Zhenping County.
Medium-carbon emission (Type II)	25	23.37	Baihe County, Chenggu County, Chunhua County, Fufeng County, Ganquan County, Hanyin County, Long County, Luonan County, Qianyang County, Shiquan County, Shanyang County, Xixiang County, Xunyi County, etc.
High-carbon emission (Type III)	68	63.55	Baishui County, Baota District, Beilin District, Binzhou City, Chang'an District, Changwu County, Chengcheng County, Chencang District, Jingbian County, Fugu County, Hengshan County, Shenmu County, etc.

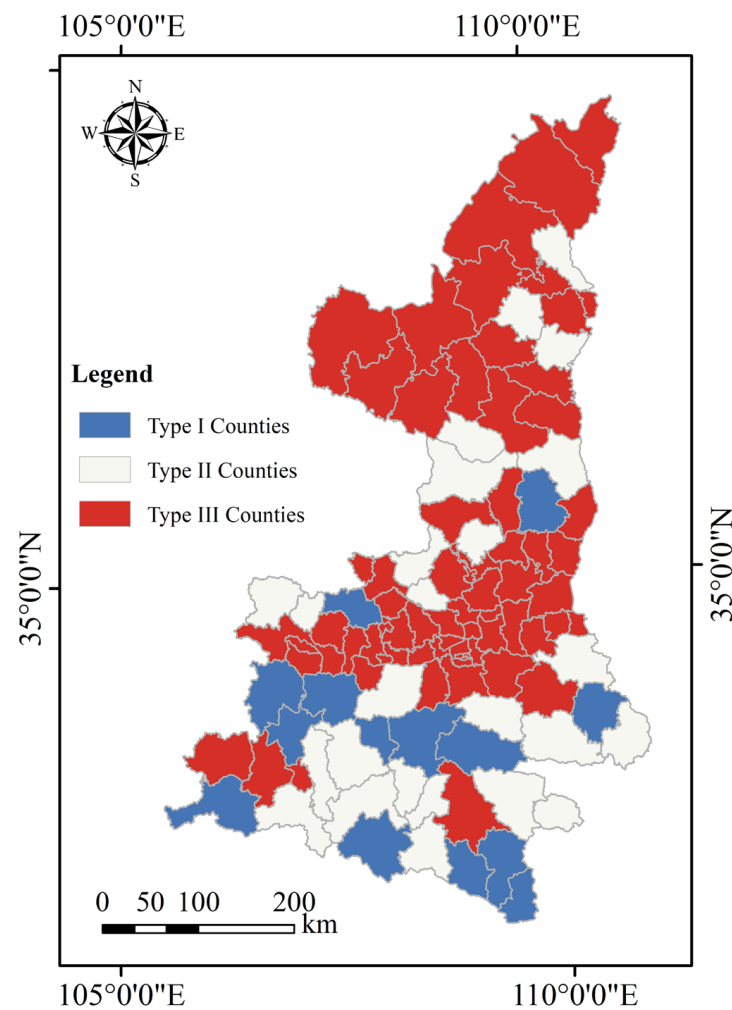


Figure 7. Clustering results of land-use carbon emissions in Shaanxi province in 2020.

The number of Type I counties was the smallest, primarily located in the southern region of Shaanxi with relatively high vegetation coverage and lower industrial activity. These counties were predominantly carbon sink regions, constituting over 85% of the total, with only Linyou County and Zhen'an County being non-carbon sink counties. Type I counties exhibited a relatively extensive original area of carbon sink land, consisting mainly of land-use types with high carbon sink coefficients, such as forest and shrubland. Owing to factors like county economic development and urban expansion, the overall carbon emissions in these counties consistently increased from 2000 to 2020, particularly notable in Feng County and Zhen'an County. The central focus of optimizing land-use carbon emissions in low-carbon emission counties involved reinforcing ecological protection and promoting rational utilization. For these countries, further pursuit of enhancing regional carbon sink capacity should involve three key aspects: ecological land-use protection, optimization of land management mechanisms, and refinement of carbon sink trading mechanisms (Table 7).

Table 7. Optimization strategies for carbon emissions in counties of different types.

Emission Type	Optimization Strategies
Low-carbon emission (Type I)	Enforce rigorous regulations to safeguard ecological land use, preventing the transformation of carbon sink land into non-carbon sink land. Optimize land management systems to sustain and enhance the carbon sequestration capabilities of currently established carbon sink zones. Improve carbon sink trading mechanisms to encourage and promote the expansion of the carbon sink industry.
Medium-carbon emission (Type II)	Optimize the industrial structure to direct industrial layouts toward green and low-carbon transitions. Plan and implement ecological corridors to enhance the integrity and connectivity of existing carbon sink areas. Enhance land-use efficiency, fostering conservation-oriented and intensive land utilization.
High-carbon emission (Type III)	Encourage the development and utilization of green energy to build a low-carbon and efficient energy supply system. Promote the conversion of some non-carbon sink lands into carbon sink lands, optimizing the regional ecological spatial structure. Implement stringent carbon emission standards and establish a comprehensive reward-penalty system for carbon emissions.

Type II counties comprised a total of 25, accounting for 23.37%, with an overall distribution pattern that was relatively dispersed. Differently from the remaining two types, type II counties displayed a relatively even distribution between carbon sink and carbon emission land-use categories, despite their spatial distribution being more scattered. Optimization strategies for counties with moderate carbon emissions should prioritize the harmonization of economic development and environmental protection. For these counties, efforts should be directed at upgrading industrial structures, improving connectivity among carbon sink lands, and enhancing land-use efficiency to promote the reduction of carbon emissions and increase carbon sink in land use (Table 7).

Type III counties were the most numerous and concentrated, representing 63.55% of the total distribution and predominantly situated in the Guanzhong and Shanbei areas. The Shaanbei region boasts abundant coal and petroleum resources and has a significant concentration of energy-intensive chemical industries. In contrast, the Guanzhong area features a high population density and a more advanced economy. As these economies advanced through industrialization, the pivotal forces governing land-use transitions stemmed from the market forces of land commodities/services and the relative economic gains associated with distinct land uses. This led to a marked shift of land towards more economically productive secondary and tertiary industries, which in turn precipitated a swift contraction of ecological habitats, idle lands, and agricultural areas, thus giving rise

to a dramatic escalation in carbon emissions. For counties characterized by high carbon emissions, optimization strategies should focus on deep emission reduction and structural transformation. When addressing the issues in these counties, measures should be taken to optimize land-use patterns and associated carbon emissions, including the development of green energy sources, conversion of land-use types into carbon sink lands, and the implementation of carbon emission reward and penalty systems (Table 7).

5.2. Advantages and Limitations of Research

This study disclosed profound alterations in land-use patterns within Shaanxi Province between 2000 and 2020, most notably an accelerated expansion of construction land, culminating in a substantial surge of carbon emissions. This aligns with the findings of Zhao et al. [62] and Wei et al. [63]. Additionally, the data from this study also demonstrated that Shaanxi Province acted as an overall carbon source region, a notion supported by Cai et al. [64] in their analysis of carbon emission characteristics in northern provinces of China. Additionally, they highlighted that industrialization and urban growth constituted the primary origins of carbon emissions, particularly within the northern counties. This study further refined these findings, focusing on elucidating the distinctive spatial variations in carbon emissions at the county scale and exploring the intricate interplay among multiple influential factors. To address these issues, this study proposed differentiated optimization strategies, echoing the call for region-specific low-carbon development strategies made by Balta-Ozkan et al. [65] in their research. Moreover, this study placed special emphasis on formulating suitable management measures according to the unique carbon emission characteristics of different counties, a topic relatively under-emphasized in previous studies, possibly due to an overarching focus on macroscale research. In summary, the study underscored the intricate relationship between alterations in land use and carbon emissions observed at the county scale. The regional analysis and recommendations reflected in this study signaled a new trend in scientific literature, shifting carbon management from a macro-policy framework towards more detailed and targeted local interventions. This not only offered a fresh perspective for theoretical studies but also provided more effective strategies for achieving sustainable low-carbon objectives in practice.

Although our research focused on Shaanxi Province, the results have potential international reference value. Globally, many countries and regions also face challenges in land-use and carbon-emission management, especially under carbon reduction targets, how to develop tailored land-use optimization strategies is particularly critical. The theoretical framework of this study can provide practical reference for other countries and regions, helping them scientifically assess the current status of land-use carbon emissions, rationally divide region types, and design targeted carbon emission optimization pathways. Nevertheless, this study also has certain shortcomings, for instance, it did not fully explore the potential challenges and solutions that different strategies may encounter during implementation. Future research could expand to more detailed scales, such as the township level, and explore the adaptability and effectiveness of different strategies under various stages of development and environmental conditions.

6. Conclusions

This study conducted an in-depth investigation of land use in 107 counties in Shaanxi Province, revealing the spatiotemporal effects and optimization strategies for land-use carbon emissions at the county level. The results demonstrated the following: (1) From 2000 to 2020, significant spatiotemporal changes occurred in land use in Shaanxi Province. Construction land, forest, shrubland, and water exhibited increasing trends, with construction land experiencing the most significant growth, expanding by 97.62%. Conversely, cultivated land, grassland, wetland, and bareland decreased, with both cultivated land and grassland experiencing a cumulative reduction of over 1500 km² each. Cultivated land, forest, and grassland dominated the provincial land composition, with prominent transitions occurring among them and construction land. Cultivated land predominantly shifted

to construction land, especially in the urbanizing regions of the Guanzhong Plain and Han River Basin. Forest mainly resulted from the conversion of grassland and cultivated land, contributing to 98.69% of forest expansion. (2) From a carbon emission perspective, Shaanxi Province acted as an overall carbon source region, demonstrating a spatial pattern of higher emissions in the northern counties, followed by the central and then southern areas. From 2000 to 2020, driven primarily by the continuous expansion of construction land, the total carbon emissions within the province increased nearly fourfold, reaching 1.00×10^8 tons. Forest played a vital role as the main carbon sink area, contributing positively to regional carbon balance. The spatial distribution of county-level carbon emissions was significantly influenced by the interaction of various factors. (3) Differentiated optimization strategies were recommended for counties with distinct carbon emission profiles: low-emission counties should enhance ecological conservation and rational land use, improving carbon sink capacities; mid-emission counties need to balance economic development and environmental protection, promoting industrial structure upgrades and enhancing land-use efficiency; and high-emission counties should prioritize deep emission reduction and structural transformation, fostering green energy development, protecting and expanding carbon sink lands, and implementing carbon emission reward and penalty systems. The research findings carry profound theoretical and practical implications for strengthening carbon emission management and optimization at the county level, thereby supporting regional carbon reduction efforts. Furthermore, they provide a scientific foundation for achieving low-carbon transition and sustainable development under the framework of dual carbon objectives.

Author Contributions: Conceptualization, Y.Z.; methodology, Y.Z. and J.Z.; software, J.L. and S.L.; formal analysis, J.L. and J.Z.; writing—original draft, Y.Z.; writing—review and editing, Y.Z., J.L., S.L. and J.Z.; funding acquisition, Y.Z. All authors have read and agreed to the published version of the manuscript.

Funding: This research was supported by the Gansu Province Longyuan Youth Innovation and Entrepreneurship Talent Plan Project, the Construction Science and Technology Project Plan of Gansu Province (JK2023-19) (Research on the Protection and Regeneration Utilization of Traditional Villages in Northwest China from the Perspective of Rural Revitalization and Social Ecological Resilience), the Science and Technology Plan Project of Gansu Province (22JR4ZA103) and the Construction Science and Technology Project Plan of Gansu Province (JK2024-25).

Data Availability Statement: Table 1 lists the access URLs for all the foundational data used in this study.

Acknowledgments: The successful completion of this study was significantly facilitated by a vast array of data sources, for which we are immensely grateful. Although we cannot feasibly itemize every data provider in this context, we extend our sincere gratitude to the numerous organizations, establishments, and persons who contributed the essential data.

Conflicts of Interest: Author Yahui Zhang was employed by the company Gansu Institute of Architectural Design and Research Co., Ltd. Authors Jianfeng Li and Siqi Liu were employed by the company Shaanxi Provincial Land Engineering Construction Group Co., Ltd. The remaining authors declare that the research was conducted in the absence of any commercial or financial relationships that could be construed as a potential conflict of interest.

References

1. Hoegh-Guldberg, O.; Jacob, D.; Taylor, M.; Guillén Bolaños, T.; Bindi, M.; Brown, S.; Camilloni, I.A.; Diedhiou, A.; Djalante, R.; Ebi, K. The human imperative of stabilizing global climate change at 1.5 C. *Science* **2019**, *365*, eaaw6974. [[CrossRef](#)]
2. Mora, C.; McKenzie, T.; Gaw, I.M.; Dean, J.M.; von Hammerstein, H.; Knudson, T.A.; Setter, R.O.; Smith, C.Z.; Webster, K.M.; Patz, J.A. Over half of known human pathogenic diseases can be aggravated by climate change. *Nat. Clim. Chang.* **2022**, *12*, 869–875. [[CrossRef](#)]
3. Mora, C.; Spirandelli, D.; Franklin, E.C.; Lynham, J.; Kantar, M.B.; Miles, W.; Smith, C.Z.; Freil, K.; Moy, J.; Louis, L.V. Broad threat to humanity from cumulative climate hazards intensified by greenhouse gas emissions. *Nat. Clim. Chang.* **2018**, *8*, 1062–1071. [[CrossRef](#)]

4. Walsh, J.E.; Ballinger, T.J.; Euskirchen, E.S.; Hanna, E.; Mård, J.; Overland, J.E.; Tangen, H.; Vihma, T. Extreme weather and climate events in northern areas: A review. *Earth-Sci. Rev.* **2020**, *209*, 103324. [[CrossRef](#)]
5. Ridder, N.; Ukkola, A.; Pitman, A.; Perkins-Kirkpatrick, S. Increased occurrence of high impact compound events under climate change. *npj Clim. Atmos. Sci.* **2022**, *5*, 3. [[CrossRef](#)]
6. Zhao, X.; Ma, X.; Chen, B.; Shang, Y.; Song, M. Challenges toward carbon neutrality in China: Strategies and countermeasures. *Resour. Conserv. Recycl.* **2022**, *176*, 105959. [[CrossRef](#)]
7. Fekete, H.; Kuramochi, T.; Roelfsema, M.; den Elzen, M.; Forsell, N.; Höhne, N.; Luna, L.; Hans, F.; Sterl, S.; Olivier, J. A review of successful climate change mitigation policies in major emitting economies and the potential of global replication. *Renew. Sustain. Energy Rev.* **2021**, *137*, 110602. [[CrossRef](#)]
8. Liu, Z.; Han, L.; Liu, M. Spatiotemporal characteristics of carbon emissions in Shaanxi, China, during 2012–2019: A machine learning method with multiple variables. *Environ. Sci. Pollut. Res.* **2023**, *30*, 87535–87548. [[CrossRef](#)]
9. Khan, I.; Lei, H.; Muhammad, I.; Khan, A.; Lei, M. Do changes in land use, water bodies, and grazing pastures have a detrimental influence on environmental quality? Opportunities and threats to long-term growth. *J. Environ. Manag.* **2023**, *325*, 116609. [[CrossRef](#)]
10. Sun, Y.; Wu, Y.; Yu, H.; Li, Y. County-level urban forms and their correlation with local governance in Jiande, China: Evidence from historical records. *J. Asian Archit. Build. Eng.* **2024**, 1–14. [[CrossRef](#)]
11. Wang, L. Assessment of land use change and carbon emission: A Log Mean Divisa (LMDI) approach. *Heliyon* **2024**, *10*, e25669. [[CrossRef](#)]
12. Kang, J.; Zhang, B.; Dang, A. A novel geospatial machine learning approach to quantify non-linear effects of land use/land cover change (LULCC) on carbon dynamics. *Int. J. Appl. Earth Obs. Geoinf.* **2024**, *128*, 103712. [[CrossRef](#)]
13. Chen, X.; Yu, L.; Hou, S.; Liu, T.; Li, X.; Li, Y.; Du, Z.; Li, C.; Wu, H.; Gao, G. Unraveling carbon stock dynamics and their determinants in China's Loess Plateau over the past 40 years. *Ecol. Indic.* **2024**, *159*, 111760. [[CrossRef](#)]
14. Padilla, F.M.; Vidal, B.; Sánchez, J.; Pugnaire, F.I. Land-use changes and carbon sequestration through the twentieth century in a Mediterranean mountain ecosystem: Implications for land management. *J. Environ. Manag.* **2010**, *91*, 2688–2695. [[CrossRef](#)]
15. Zhang, X.; Fan, H.; Hou, H.; Xu, C.; Sun, L.; Li, Q.; Ren, J. Spatiotemporal evolution and multi-scale coupling effects of land-use carbon emissions and ecological environmental quality. *Sci. Total Environ.* **2024**, *922*, 171149. [[CrossRef](#)]
16. Liu, G.; Cui, F.; Wang, Y. Spatial effects of urbanization, ecological construction and their interaction on land use carbon emissions/absorption: Evidence from China. *Ecol. Indic.* **2024**, *160*, 111817. [[CrossRef](#)]
17. Zhang, C.-y.; Zhao, L.; Zhang, H.; Chen, M.-n.; Fang, R.-y.; Yao, Y.; Zhang, Q.-P.; Wang, Q. Spatial-temporal characteristics of carbon emissions from land use change in Yellow River Delta region, China. *Ecol. Indic.* **2022**, *136*, 108623. [[CrossRef](#)]
18. Hunter, M.L.; Clark, L.; Frei, R.J.; Strachan, I.B.; Roulet, N.T.; Strack, M. Carbon Emissions from Active Horticulture Peat Extraction Sites in Canada: Five Years of Field-based Measurements. In Proceedings of the Copernicus Meetings, Vienna, Austria & Online, 14–19 April 2024.
19. Li, S.; Yao, L.; Zhang, Y.; Zhao, Y.; Sun, L. China's Provincial Carbon Emission Driving Factors Analysis and Scenario Forecasting. *Environ. Sustain. Indic.* **2024**, *22*, 100390. [[CrossRef](#)]
20. Lawrence, P.J.; Lawrence, D.M.; Hurtt, G.C. Attributing the carbon cycle impacts of CMIP5 historical and future land use and land cover change in the Community Earth System Model (CESM1). *J. Geophys. Res. Biogeosci.* **2018**, *123*, 1732–1755. [[CrossRef](#)]
21. Bovensmann, H.; Buchwitz, M.; Burrows, J.; Reuter, M.; Krings, T.; Gerilowski, K.; Schneising, O.; Heymann, J.; Tretner, A.; Erzinger, J. A remote sensing technique for global monitoring of power plant CO₂ emissions from space and related applications. *Atmos. Meas. Tech.* **2010**, *3*, 781–811. [[CrossRef](#)]
22. Tang, X.; Zhao, X.; Bai, Y.; Tang, Z.; Wang, W.; Zhao, Y.; Wan, H.; Xie, Z.; Shi, X.; Wu, B. Carbon pools in China's terrestrial ecosystems: New estimates based on an intensive field survey. *Proc. Natl. Acad. Sci. USA* **2018**, *115*, 4021–4026. [[CrossRef](#)]
23. Jiang, Y.; Zhao, R.; Qin, G. How does digital finance reduce carbon emissions intensity? Evidence from chain mediation effect of production technology innovation and green technology innovation. *Heliyon* **2024**, *10*, e30155. [[CrossRef](#)]
24. Liu, C.; Hu, S.; Wu, S.; Song, J.; Li, H. County-Level Land Use Carbon Emissions in China: Spatiotemporal Patterns and Impact Factors. *Sustain. Cities Soc.* **2024**, *105*, 105304. [[CrossRef](#)]
25. Duman, Z.; Mao, X.; Cai, B.; Zhang, Q.; Chen, Y.; Gao, Y.; Guo, Z. Exploring the spatiotemporal pattern evolution of carbon emissions and air pollution in Chinese cities. *J. Environ. Manag.* **2023**, *345*, 118870. [[CrossRef](#)]
26. Van Vuuren, D.P.; Stehfest, E.; Gernaat, D.E.; Doelman, J.C.; Van den Berg, M.; Harmsen, M.; de Boer, H.S.; Bouwman, L.F.; Daioglou, V.; Edelenbosch, O.Y. Energy, land-use and greenhouse gas emissions trajectories under a green growth paradigm. *Glob. Environ. Chang.* **2017**, *42*, 237–250. [[CrossRef](#)]
27. Zhang, X.; Zhang, D. Urban carbon emission scenario prediction and multi-objective land use optimization strategy under carbon emission constraints. *J. Clean. Prod.* **2023**, *430*, 139684. [[CrossRef](#)]
28. Huisingh, D.; Zhang, Z.; Moore, J.C.; Qiao, Q.; Li, Q. Recent advances in carbon emissions reduction: Policies, technologies, monitoring, assessment and modeling. *J. Clean. Prod.* **2015**, *103*, 1–12. [[CrossRef](#)]
29. Ding, S.; Liu, S.; Chang, M.; Lin, H.; Lv, T.; Zhang, Y.; Zeng, C. Spatial Optimization of Land Use Pattern toward Carbon Mitigation Targets—A Study in Guangzhou. *Land* **2023**, *12*, 1903. [[CrossRef](#)]
30. An, Q.; Zheng, L.; Yang, M. Spatiotemporal Heterogeneities in the Impact of Chinese Digital Economy Development on Carbon Emissions. *Sustainability* **2024**, *16*, 2810. [[CrossRef](#)]

31. Tang, X.; Woodcock, C.E.; Olofsson, P.; Hutyrá, L.R. Spatiotemporal assessment of land use/land cover change and associated carbon emissions and uptake in the Mekong River Basin. *Remote Sens. Environ.* **2021**, *256*, 112336. [[CrossRef](#)]
32. Qin, J.; Duan, W.; Zou, S.; Chen, Y.; Huang, W.; Rosa, L. Global energy use and carbon emissions from irrigated agriculture. *Nat. Commun.* **2024**, *15*, 3084. [[CrossRef](#)]
33. Cheng, Y.; Tang, Y.; Zhou, B.; Feng, H. Spatiotemporal analysis of national carbon emission and regional carbon simulation in China. *Environ. Sci. Pollut. Res.* **2024**, *31*, 10702–10716. [[CrossRef](#)]
34. Wang, Y.; Wang, W.; Chen, Y.; Wu, L. Projection of ecological water consumption under carbon emission in Chinese provinces. *J. Clean. Prod.* **2024**, *448*, 141630. [[CrossRef](#)]
35. Chen, Y.; Lu, H.; Li, J.; Xia, J. Effects of land use cover change on carbon emissions and ecosystem services in Chengyu urban agglomeration, China. *Stoch. Environ. Res. Risk Assess.* **2020**, *34*, 1197–1215. [[CrossRef](#)]
36. Carpio, A.; Ponce-Lopez, R.; Lozano-García, D.F. Urban form, land use, and cover change and their impact on carbon emissions in the Monterrey Metropolitan area, Mexico. *Urban Clim.* **2021**, *39*, 100947. [[CrossRef](#)]
37. Rivera-Niquepa, J.D.; Rojas-Lozano, D.; De Oliveira-De Jesus, P.M.; Yusta, J.M. Methodology for selecting assessment periods of Logarithmic Mean Divisia Index decomposition techniques. *Energy Strategy Rev.* **2023**, *50*, 101241. [[CrossRef](#)]
38. Aziz, S.; Chowdhury, S.A. Analysis of agricultural greenhouse gas emissions using the STIRPAT model: A case study of Bangladesh. *Environ. Dev. Sustain.* **2023**, *25*, 3945–3965. [[CrossRef](#)]
39. Rehman, E.; Rehman, S. Modeling the nexus between carbon emissions, urbanization, population growth, energy consumption, and economic development in Asia: Evidence from grey relational analysis. *Energy Rep.* **2022**, *8*, 5430–5442. [[CrossRef](#)]
40. Liang, Y.; Xu, C. Knowledge diffusion of Geodetector: A perspective of the literature review and Geotree. *Heliyon* **2023**, *9*, e19651. [[CrossRef](#)] [[PubMed](#)]
41. Rahman, M.M.; Szabó, G. Multi-objective urban land use optimization using spatial data: A systematic review. *Sustain. Cities Soc.* **2021**, *74*, 103214. [[CrossRef](#)]
42. Kongsager, R. Linking climate change adaptation and mitigation: A review with evidence from the land-use sectors. *Land* **2018**, *7*, 158. [[CrossRef](#)]
43. Zhang, K.; Wang, S.; Bao, H.; Zhao, X. Characteristics and influencing factors of rainfall-induced landslide and debris flow hazards in Shaanxi Province, China. *Nat. Hazards Earth Syst. Sci.* **2019**, *19*, 93–105. [[CrossRef](#)]
44. Tatem, A.J. WorldPop, open data for spatial demography. *Sci. Data* **2017**, *4*, 1–4. [[CrossRef](#)]
45. Chen, Z.; Yu, B.; Yang, C.; Zhou, Y.; Yao, S.; Qian, X.; Wang, C.; Wu, B.; Wu, J. An extended time series (2000–2018) of global NPP-VIIRS-like nighttime light data from a cross-sensor calibration. *Earth Syst. Sci. Data* **2021**, *13*, 889–906. [[CrossRef](#)]
46. Huang, Y.; Jiang, D.; Fu, J. China km grid GDP distribution data set. *Glob. Chang. Sci. Res. Data* **2014**, *1*, 5–8.
47. Oda, T.; Maksyutov, S.; Andres, R.J. The Open-source Data Inventory for Anthropogenic CO₂, version 2016 (ODIAC2016): A global monthly fossil fuel CO₂ gridded emissions data product for tracer transport simulations and surface flux inversions. *Earth Syst. Sci. Data* **2018**, *10*, 87–107. [[CrossRef](#)]
48. Xie, X.; Deng, H.; Li, S.; Gou, Z. Optimizing Land Use for Carbon Neutrality: Integrating Photovoltaic Development in Lingbao, Henan Province. *Land* **2024**, *13*, 97. [[CrossRef](#)]
49. Lamb, W.F.; Wiedmann, T.; Pongratz, J.; Andrew, R.; Crippa, M.; Olivier, J.G.; Wiedenhofer, D.; Mattioli, G.; Al Khourdajie, A.; House, J. A review of trends and drivers of greenhouse gas emissions by sector from 1990 to 2018. *Environ. Res. Lett.* **2021**, *16*, 073005. [[CrossRef](#)]
50. Wu, H.; Zheng, X.; Zhou, L.; Meng, Y. Spatial autocorrelation and driving factors of carbon emission density of crop production in China. *Environ. Sci. Pollut. Res.* **2024**, *31*, 27172–27191. [[CrossRef](#)] [[PubMed](#)]
51. Tian, S.; Wang, S.; Bai, X.; Luo, G.; Li, Q.; Yang, Y.; Hu, Z.; Li, C.; Deng, Y. Global patterns and changes of carbon emissions from land use during 1992–2015. *Environ. Sci. Ecotechnol.* **2021**, *7*, 100108. [[CrossRef](#)] [[PubMed](#)]
52. Fang, J.; Yu, G.; Liu, L.; Hu, S.; Chapin III, F.S. Climate change, human impacts, and carbon sequestration in China. *Proc. Natl. Acad. Sci. USA* **2018**, *115*, 4015–4020. [[CrossRef](#)] [[PubMed](#)]
53. Chen, H.; Zhou, S.; Wu, N.; Wang, Y.; Luo, P.; Shi, F. Advance in studies on production, oxidation and emission flux of methane from wetlands. *Chin. J. Appl. Environ. Biol.* **2006**, *12*, 726.
54. Sun, H.; Liang, H.; Chang, X.; Cui, Q.; Tao, Y. Land use patterns on carbon emission and spatial association in China. *Econ. Geogr.* **2015**, *35*, 154–162.
55. Lin, Q.; Zhang, L.; Qiu, B.; Zhao, Y.; Wei, C. Spatiotemporal analysis of land use patterns on carbon emissions in China. *Land* **2021**, *10*, 141. [[CrossRef](#)]
56. Likas, A.; Vlassis, N.; Verbeek, J.J. The global k-means clustering algorithm. *Pattern Recognit.* **2003**, *36*, 451–461. [[CrossRef](#)]
57. Ma, X.; Zhao, C.; Song, C.; Meng, D.; Xu, M.; Liu, R.; Yan, Y.; Liu, Z. The impact of regional policy implementation on the decoupling of carbon emissions and economic development. *J. Environ. Manag.* **2024**, *355*, 120472. [[CrossRef](#)]
58. Bao, H.; Tao, H.; Zhuo, L.; Shi, Q.; Guo, S. Estimation of Economic Spillover Effects under the Hierarchical Structure of Urban Agglomeration Based on Time-Series Night-Time Lights: A Case Study of the Pearl River Delta, China. *Remote Sens.* **2024**, *16*, 394. [[CrossRef](#)]
59. Huang, S.; Yu, L.; Cai, D.; Zhu, J.; Liu, Z.; Zhang, Z.; Nie, Y.; Fraedrich, K. Driving mechanisms of urbanization: Evidence from geographical, climatic, social-economic and nighttime light data. *Ecol. Indic.* **2023**, *148*, 110046. [[CrossRef](#)]

60. Liang, L.; Liang, S.; Zeng, Z. Extreme climate sparks record boreal wildfires and carbon surge in 2023. *Innovation* **2024**, 100631. [[CrossRef](#)]
61. Cao, X.; Wang, H.; Zhang, B.; Liu, J.; Yang, J. Sustainable Management of Land Use Patterns and Water Allocation for Coordinated Multidimensional Development. *J. Clean. Prod.* **2024**, 142412. [[CrossRef](#)]
62. Zhao, C.; Liu, Y.; Yan, Z. Effects of land-use change on carbon emission and its driving factors in Shaanxi Province from 2000 to 2020. *Environ. Sci. Pollut. Res.* **2023**, 30, 68313–68326. [[CrossRef](#)]
63. Fang, W.; Luo, P.; Luo, L.; Zha, X.; Nover, D. Spatiotemporal characteristics and influencing factors of carbon emissions from land-use change in Shaanxi Province, China. *Environ. Sci. Pollut. Res.* **2023**, 30, 123480–123496. [[CrossRef](#)]
64. Cai, B.; Wang, X.; Huang, G.; Wang, J.; Cao, D.; Baetz, B.W.; Liu, L.; Zhang, H.; Fenech, A.; Liu, Z. Spatiotemporal changes of China's carbon emissions. *Geophys. Res. Lett.* **2018**, 45, 8536–8546. [[CrossRef](#)]
65. Balta-Ozkan, N.; Watson, T.; Mocca, E. Spatially uneven development and low carbon transitions: Insights from urban and regional planning. *Energy Policy* **2015**, 47, 500–510. [[CrossRef](#)]

Disclaimer/Publisher's Note: The statements, opinions and data contained in all publications are solely those of the individual author(s) and contributor(s) and not of MDPI and/or the editor(s). MDPI and/or the editor(s) disclaim responsibility for any injury to people or property resulting from any ideas, methods, instructions or products referred to in the content.